JOURNAL OF CATALYSIS 157, 42–50 (1995)

Redox Activity of Nonstoichiometric Cerium Oxide-Based Nanocrystalline Catalysts

Andreas Tschöpe, Wei Liu, Maria Flytzani-Stephanopoulos,* and Jackie Y. Ying[1]

*Department of Chemical Engineering, Massachusetts Institute of Technology, Cambridge, Massachusetts 02139; and *Department of Chemical Engineering, Tufts University, Medford, Massachusetts 02155*

Received August 24, 1994; revised March 30, 1995; accepted July 11, 1995

Nonstoichiometric cerium oxide-based catalysts were investigated for SO_2 reduction by CO to elemental sulfur, CO oxidation, and complete methane oxidation. Nanocrystalline processing by inert gas condensation was exploited for its unique potential to generate nonstoichiometric ultrahighly dispersed oxides. Nanocrystalline CeO_{2-x} materials, pure or doped with 10 at.% La or 15 at.% Cu, were generated by magnetron sputtering from pure or mixed metal targets, followed by controlled oxidation. These materials allowed us to investigate the effects of oxide nonstoichiometry and dopants on catalytic activity in oxidation reactions. The nonstoichiometric materials were characterized by X-ray diffraction, nitrogen adsorption porosimetry, and X-ray photoelectron spectroscopy. Catalytic properties were studied in a packed-bed reactor and compared to materials of similar composition prepared by coprecipitation. In general, the nonstoichiometric CeO_2-based materials exhibited greater catalytic activity than precipitated ultrafine materials. The light-off temperatures for SO_2 reduction by CO, CO oxidation, and CH_4 oxidation were 100–180°C lower for the nanocrystalline pure and La-doped CeO_{2-x} catalysts than for the respective precipitated materials. The Cu-doped form of both types of catalysts possessed comparable activity. The nonstoichiometric materials did not show a hysteresis behavior in the activity profile for SO_2 reduction by CO, unlike the precipitated catalysts. They further demonstrated a remarkable stability against CO_2 poisoning in this reaction. The differences between the nanocrystalline and the precipitated materials are discussed in terms of the stoichiometry of these oxide catalysts. © 1995 Academic Press, Inc.

INTRODUCTION

Catalytic oxidation reactions are extensively used for industrial synthesis of chemicals and environmental pollution control. They include partial oxidation reactions, complete combustion, and oxidative dehydrogenation. Typical oxidation catalysts are metal oxides and pure metals on which chemisorbed oxygen is the oxidizing species. With metal oxides the nature of the reacting oxygen species is less obvious. In addition to adsorbed surface species, lattice oxygen can participate in the reaction depending on the oxide used.

Catalytic oxidation reactions on metal oxides are often described in terms of a general redox mechanism:

$$\begin{aligned} \text{Cat}-\text{O} + \text{Red} &\rightarrow \text{Cat} + \text{Red}-\text{O} \\ \text{Cat} + \text{Ox}-\text{O} &\rightarrow \text{Cat}-\text{O} + \text{Ox}. \end{aligned}$$

Here, the oxide catalyst surface (Cat—O) is reduced by a reductant (Red) and reoxidized by an oxidant (Ox—O) to its initial state. The net result of this two-step reaction is the transfer of oxygen from one species to the other. Based on isotope exchange experiments, this general scheme has been divided more specifically into (i) extrafacial reactions, in which only adsorbed surface oxygen reacts and lattice oxygen does not participate in the reaction; and (ii) interfacial reactions, where lattice oxygen is extracted and oxygen vacancies are created (1). Stability of the oxide and the type of active oxygen species might also determine selectivity of the oxidation reaction. It has been proposed that redox reactions involving lattice oxygen result in the partial oxidation of hydrocarbons (nucleophilic reactions), whereas active surface species such as O_2^- lead to complete combustion products (electrophilic reactions) (1). This hypothesis suggests that designing the oxidative properties of a catalyst would require control of the nature of the active oxygen species. Oxidation properties become even more complex in the case of supported oxide catalysts. A variety of metal–support interactions can lead to synergistic effects and enhanced catalytic properties (2).

Cerium oxide is well known for its large deviation from stoichiometry at low oxygen partial pressures and temperatures above 500°C (3, 4). Easy reducibility and high mobility of oxygen vacancies in the fluorite crystal structure of CeO_2 might be the reason for high catalytic activity in redox reactions. CeO_2 doped with lower-valent cations is found to be an excellent catalyst for the direct reduction

[1] To whom correspondence should be addressed.

0021-9517/95 $12.00

of SO_2 by CO (5). For the Cu—Ce—O system, complete conversion of SO_2 and better than 95% selectivity to elemental sulfur above 500°C have been reported (6). This catalytic material was also highly active in low-temperature CO oxidation and methane oxidation (7).

The present work is focused on the change in catalytic properties with the use of nanocrystalline nonstoichiometric CeO_{2-x}-based catalysts. The defect chemistry of bulk CeO_2 is well established (8) and shows that upon reduction, oxygen vacancies are created, which are initially doubly ionized and then singly ionized at larger deviations from stoichiometry. Electrons which are released from the vacancy sites are back-donated to localized Ce_{4f} states and mobile by a small-polaron hopping process (9). Reduced CeO_{2-x} is therefore a mixed ionic/electronic conductor. The availability of quasi-free electrons is assumed to be responsible for the occurrence of surface oxygen species such as superoxide O_2^- and peroxide O_2^{2-} on reduced CeO_{2-x} (10, 11). In contrast to bulk defect chemistry, information on defect thermodynamics at CeO_2 surfaces is very limited. A recent computer simulation shows that the enthalpy of vacancy formation at the surface is considerably lower than that of the bulk and depends on the crystallography of the surface (12).

Cerium oxide prepared by precipitation from aqueous salt solution and calcination at elevated temperature is stoichiometric in nature. Attempts to reduce unsupported CeO_2 by hydrogen or carbon monoxide and achieve nonstoichiometric CeO_{2-x} are usually unsuccessful since the reduced material will be reoxidized readily when exposed to an oxidizing atmosphere. Although nonstoichiometric catalytic properties of cerium oxide have been extensively reported in the literature, no such materials that are stable under atmospheric conditions have been synthesized so far. In the present study, ultrafine nonstoichiometric CeO_{2-x} is synthesized by inert gas condensation. This method for cluster synthesis has been adapted for generating nanocrystalline pure metals and compounds (13–15). Nonstoichiometric metal oxides can be produced by first synthesizing metallic nanoclusters, followed by controlled oxidation.

Pure and doped nanocrystalline CeO_{2-x} was synthesized by magnetron sputtering and inert gas condensation. The catalytic activities of these materials in SO_2 reduction by CO, CO oxidation, and CH_4 oxidation were compared to those of conventional stoichiometric catalysts synthesized by coprecipitation. Differences in catalytic activity are discussed in terms of the nonstoichiometric nature of the nanocrystalline materials. Two possible changes in the catalyst material due to nonstoichiometry can be anticipated: (i) presence of oxygen vacancies, and (ii) availability of quasi-free electrons. The effect of these changes will become apparent in the different activities of the pure nanocrystalline CeO_{2-x} and the precipitated CeO_2. La-doping is well known to generate oxygen vacancies without liberation of electrons; thus stoichiometric La-doped CeO_2 is a pure ionic conductor (16). In nonstoichiometric $(La)CeO_{2-x}$, additional oxygen vacancies and free electrons exist simultaneously, and conductivity is mixed ionic and electronic. Hence, precipitated $(La)CeO_2$ will elucidate the effect of oxygen vacancies in the absence of free electrons, whereas nanocrystalline $(La)CeO_{2-x}$ represents a material with essentially the same chemical composition but mixed ionic/electronic conductivity.

Supported metal catalysts such as Pt or Pd on Al_2O_3 are typical catalysts for CO oxidation or methane oxidation. Due to the high cost of the precious metals, research efforts have continued over the years to develop base metal catalysts for oxidation reactions. Copper is one of the most studied base metals exhibiting high activity in methanol synthesis (17) and CO oxidation (18). The promoting effect of Cu is also investigated in the present study. The catalytic activity of nonstoichiometric Cu-doped CeO_{2-x} is compared with that of precipitated $(Cu)CeO_2$.

The main objective of these studies was to investigate the potential of designing specific surface properties through control of the nonstoichiometry of oxide catalysts.

METHODS

Nanocrystalline Ce clusters were generated in an ultrahigh vacuum (UHV) chamber by magnetron sputtering from metallic Ce targets (purity 99.99%) under a 50-Pa argon atmosphere (19, 20). This argon pressure is high enough to rapidly thermalize and supersaturate the metal vapor, leading to homogeneous nucleation of nanometer-sized clusters in the gas phase (21). A liquid-nitrogen-cooled modified ground shield was used as the substrate to collect the clusters (19). After deposition for 20 min, the UHV chamber was evacuated and slowly back-filled with oxygen to a final pressure of 100 Pa. During oxidation, the color of the deposit on the substrate changed from black to brownish-yellow. The oxidized material was then scraped off and studied in a catalytic reactor in this as-prepared powder form. For XRD and XPS studies, the clusters were consolidated in a connected UHV compaction unit to solid discs of 5 mm diameter and 1 mm thickness. A uniaxial compaction pressure of 0.5 GPa yielded self-supporting pellets with about 35% porosity. For doped nanocrystalline CeO_{2-x}, sputtering from mixed metal targets (Cu/Ce = 15/85 and La/Ce = 10/90) was undertaken. XPS analyses confirmed that average composition was maintained after the sputtering process. More details on catalyst preparation by this method can be found in Ref. (19). Sputtering has the advantage of reproducing the target composition in the samples and generating the most intimate mixture possible (19, 22). Sputtering from mixed metal targets has been used in the synthesis of Au/Co_3O_4 granular films, which yielded high activity in CO oxidation

(23). It should be noted that the inert gas condensation technique differs from the granular film sputtering technique in that for the former, cluster formation occurs in the gas phase rather than on the substrate, and the product is in a particulate, instead of thin film, form.

Stoichiometric CeO_2 was prepared by pyrolysis of cerium hydroxycarbonates that were precipitated from an aqueous solution of $Ce(NO_3)_3$ and $(NH_4)_2CO_3$ (6, 7). Doped catalysts were coprecipitated from mixed nitrate solutions by the addition of $(NH_4)_2CO_3$. The precipitate was washed in deionized water, dried at room temperature, and calcined for 4 h at 650°C in air. These samples were used as stoichiometric reference materials.

The nonstoichiometric and stoichiometric cerium oxide samples were characterized by XRD (Rigaku rotating anode powder diffractometer) and nitrogen adsorption (Micromeritics ASAP 2000). The (111) and (222) XRD peak widths of CeO_2 were determined by a least-square fit of a Cauchy function. Deconvolution of the instrumental line broadening yielded the physical peak width. Kochendorfer analysis (24) and the Scherrer equation (25) were then applied to calculate the mean crystal size of the CeO_{2-x} particles, corrected for internal strain contributions. The specific surface area was obtained from 5-point BET analysis of nitrogen adsorption experiments. The oxidation state of the nonstoichiometric materials was analyzed with the Ce_{3d} core level spectra obtained from XPS (Perkin–Elmer PHI-5500) (26). The XPS spectrometer was connected to a reaction chamber in which the sample could be oxidized at elevated temperatures. The sample was transferred to the XPS analysis chamber without exposure to ambient atmosphere.

Catalytic testing was performed in a packed-bed microreactor under continuous gas flow. A sample of 50–150 mg was supported on a quartz frit in a quartz tube reactor (6 mm diameter) heated by a Lindberg furnace. Reactants (CO, CH_4, SO_2) were all certified calibration gas mixtures balanced by helium (from Matheson). Air and helium (from AIRCO) were used as oxidizing gas and diluting medium, respectively. Stoichiometric gas composition (1% SO_2/2% CO) was used for SO_2 reduction by CO, while 2% CO/16% O_2 and 2% CH_4/16% O_2 were used for CO oxidation and methane oxidation, respectively. Without further purification the gas mixture was passed over the catalyst bed at a flow rate of 50–100 sccm. The typical contact time was 0.09 s · g/cc (STP). The composition of the effluent gas was analyzed by a HP-5880A gas chromatograph equipped with a thermal conductivity detector. The activity measurements were conducted under steady-state reaction conditions. The catalytic activities were compared based on the light-off temperature at which 50% conversion was achieved. More details about the experimental setup and procedures can be found in Refs. (5–7).

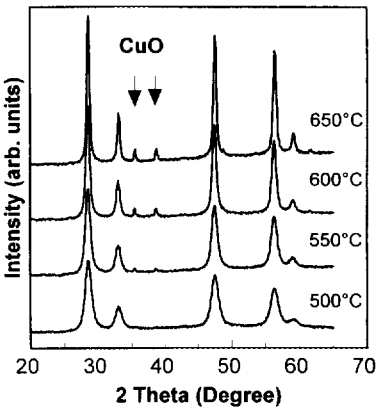

FIG. 1. XRD pattern of nonstoichiometric Cu-doped CeO_{2-x} after oxidation in 15% O_2/He at the indicated temperatures.

RESULTS

Microstructure and Stoichiometry

All materials in this study gave the cubic XRD pattern of the fluorite crystal structure of CeO_2. Cu-doped nanocrystalline CeO_{2-x} underwent interesting microstructural evolution after heat treatments. Nanocrystalline Cu/CeO_{2-x} was annealed at increasing temperatures for 10 h under 15% O_2/He. After being annealed at 500°C, the XRD of this sample still only consisted of the cubic pattern of the fluorite structure (Fig. 1) (19). At 550°C and higher temperatures, the CuO phase appeared, accompanied by the grain growth of CeO_{2-x} particles (indicated by the sharpening of the diffraction peaks). The binary metallic phase diagram indicates that Cu and Ce form intermetallic phases (27). Magnetron sputtering from a mixed metal target should yield a well-mixed solid solution of metallic Cu and Ce. Although there is no ternary phase diagram of Cu—Ce—O to our knowledge, it may be assumed that Cu has very limited solubility in CeO_2 (as in ZrO_2), due to the large difference in ionic radius. Therefore, oxidation will force Cu to segregate to the surface and eventually form a secondary phase. This process is clearly revealed by XRD. Precipitation of a Cu phase from CeO_2 is in accordance with previous studies on intermetallic $CeCu_2$, which was used as catalyst for methanol synthesis (28). The CuO phase was visible in the as-prepared coprecipitated and 650°C-calcined Cu—Ce—O sample, depending on the preparation conditions. It is noteworthy that the crystallite size of cerium oxide did not differ much between the two preparations; namely ~8 nm and 8~14 nm (7) for the materials prepared by the gas condensation and the coprecipitation with 650°C air calcination, respectively.

The specific BET surface areas were 50–65 m^2/g for the materials as generated by the inert gas condensation, and 25–45 m^2/g for the coprecipitated/650°C-calcined catalysts. The thermal stability of the nanocrystalline materials was

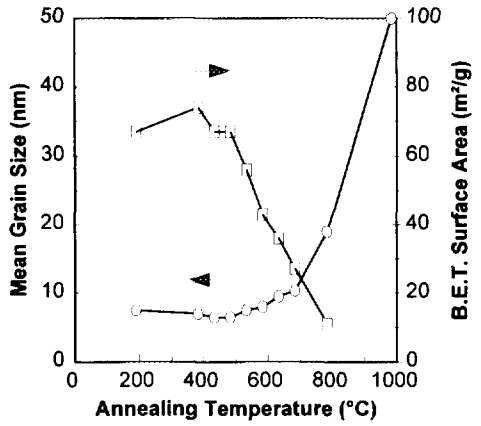

FIG. 2. Mean grain size and BET surface area of nonstoichiometric La-doped CeO_{2-x} after being annealed for 10 h under 15% O_2/He at the indicated temperatures.

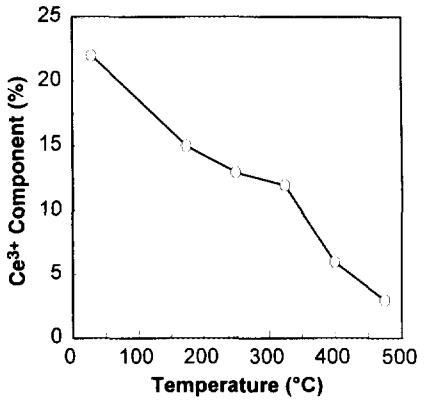

FIG. 4. Percentage of Ce^{3+} component determined by deconvolution of the Ce_{3d} core level spectrum after being annealed under 1 kPa of 1% CO_2/He at the temperatures indicated.

investigated by measuring grain growth and sintering as a function of heat treatments for 10 h at increasing temperatures (Fig. 2). Grain growth and sintering of nanocrystalline samples were initiated above 500°C, and after being annealed at 650°C these materials became comparable in surface area to the precipitated samples which were calcined for 4 h at the same temperature. Annealing of the La-doped CeO_{2-x} in oxygen flow saturated with water vapor at 80°C showed that sintering was not affected by the presence of moisture. A reaction temperature of 650°C is the upper limit for all catalytic studies in this report.

XPS was employed to investigate the oxidation state of the nonstoichiometric materials and their stability against oxidation. The Ce_{3d} core level spectrum of CeO_2 exhibits 6 lines, denoted v, v″, v‴, u, u″, and u‴ (29, 30). As-prepared nonstoichiometric CeO_{2-x} showed two additional lines, v′ and u′ (Fig. 3). These peaks were also found in hydrogen-reduced CeO_2 and were due to Ce cations in the initial oxidation state of +3 (26, 31). After oxidation at 500°C under 1 kPA of 1% CO_2/He, these peaks were no longer observed. In order to study the oxidation process, nanocrystalline CeO_{2-x} was annealed at increasing temperatures in 1 kPa of 1% CO_2/He in the reaction chamber connected to the XPS system. Deconvolution of the spectrum into the different components can be used to determine the percentage of Ce^{3+} (26, 30, 31). As a result of the oxidation, the Ce^{3+} component decreased gradually, as shown in Fig. 4.

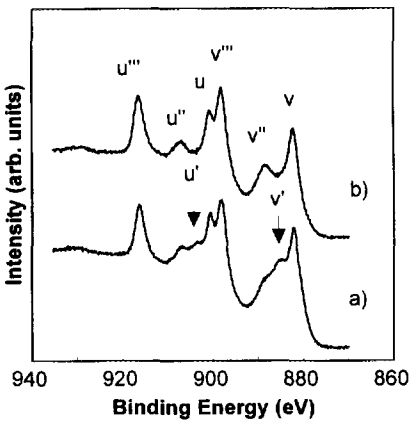

FIG. 3. XPS Ce_{3d} core level spectra for nonstoichiometric CeO_{2-x}: (a) as-prepared, and (b) after oxidation under 1 kPa of 1% CO_2/He at 475°C.

SO_2 Reduction by CO

The two possible reactions which can be anticipated in this case are the reduction of SO_2 to elemental S

$$2\,CO + SO_2 \rightarrow 2\,CO_2 + S \qquad [1]$$

and the formation of COS from adsorbed S and CO

$$[S] + CO \rightarrow COS. \qquad [2]$$

Since COS is a highly toxic compound, high selectivity to elemental sulfur is crucial. High selectivity toward elemental sulfur and low COS formation was obtained for all CeO_2-based catalysts (5, 6).

A typical activity profile for this reaction is shown in Fig. 5 for coprecipitated 10 at.% La-doped CeO_2 (6). The sulfur yield, which is the ratio of elemental sulfur produced to the initial SO_2 in the feed, increased rapidly above 550°C to more than 95%. After activation, the reaction temperature could be reduced to 500°C without any loss of activity until the sulfur yield falls off below 500°C. This process gave rise to a hysteresis loop in the activity profile. It was found that the light-off and fall-off temperatures for this reaction were independent of contact time above a certain

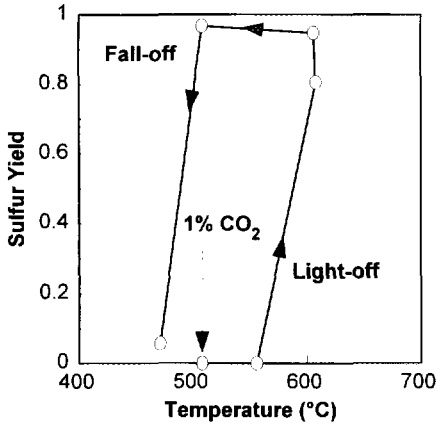

FIG. 5. Catalytic activity profile for SO_2 reduction by CO over precipitated La-doped CeO_2 with light-off and fall-off behavior. The effect of CO_2 poisoning is also indicated.

critical value (ca. 0.045 s · g/cc) (5, 6). Therefore, these temperatures are a measure for intrinsic kinetic limitations in the catalytic process.

Catalytic activities of nonstoichiometric and precipitated CeO_2-based catalysts were compared in terms of their light-off and fall-off temperatures corresponding to 50% conversion (Fig. 6). The two main results for the nonstoichiometric cerium oxide catalysts were (i) their higher activity than those of the respective precipitated materials, and (ii) their much smaller hysteresis behavior (32). The light-off temperature of nonstoichiometric CeO_{2-x} was at 460°C, which was 120°C lower than for precipitated CeO_2, and hysteresis was reduced from 80 to 25°C. La-doping did not improve the catalytic activity in terms of the light-off temperature. The fall-off temperatures for Cu-doped CeO_2 catalysts were similar for both types of materials. However, the nonstoichiometric sample again showed a much smaller hysteresis.

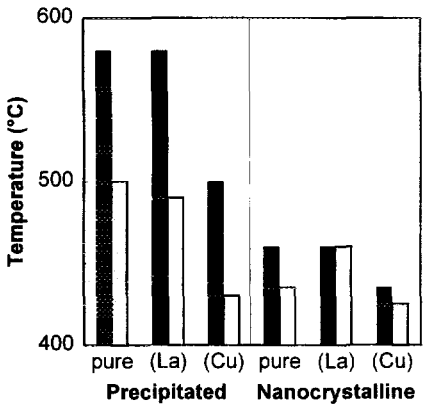

FIG. 6. Light-off (full bars) and fall-off (open bars) temperatures of precipitated and nanocrystalline nonstoichiometric cerium oxide catalysts for SO_2 reduction by CO at 50% conversion.

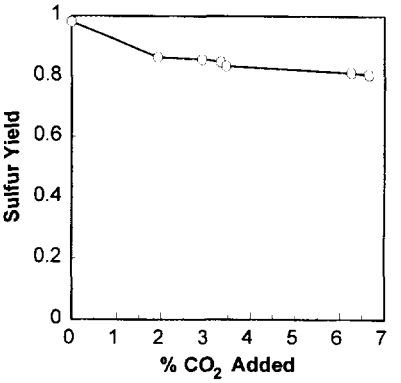

FIG. 7. Sulfur yield of nonstoichiometric La-doped CeO_{2-x} as a function of % CO_2 added to the feed gas mixture at 515°C.

The effect of excess CO_2 in the feed gas is also depicted in Fig. 5. The precipitated La-doped CeO_2 catalyst that was active at 510°C became completely deactivated by the addition of 1% CO_2. The entire 2% CO feed concentration was detected in the effluent gas. Hence, the result of poisoning was that CO could no longer reduce the surface at this temperature. The catalyst had to be heated to the light-off temperature in order to be reactivated. La-doped CeO_{2-x} was more tolerant to CO_2. Thus, the sulfur yield decreased only slightly to 80% and remained high even at a CO_2 concentration of 6.5% in the feed gas containing 1% SO_2 and 2% CO (Fig. 7).

CO Oxidation by O_2

$$2\,CO + O_2 \rightarrow 2\,CO_2 \qquad [3]$$

Neither nonstoichiometric nor precipitated CeO_2 catalysts exhibit a hysteresis behavior in the activity profile for this reaction. Similar to the SO_2 reduction by CO, CO oxidation light-off temperature over the CeO_2-based catalyst was not affected by contact time and gas composition. The light-off temperature of 400°C for precipitated stoichiometric CeO_2 was considerably lowered to ~200°C with the use of nonstoichiometric pure and La-doped CeO_{2-x} (Fig. 8). Although the La-doped CeO_{2-x} had a light-off temperature similar to that of the pure CeO_{2-x}, the CO conversion profile versus temperature leveled off more rapidly at high conversions on the La-doped CeO_{2-x} than on the pure CeO_{2-x}. The most active catalyst in this study was again the Cu-doped cerium oxide with a light-off temperature of 80°C for both types of materials (Fig. 9).

CH_4 Oxidation by O_2

$$CH_4 + 2\,O_2 \rightarrow CO_2 + 2\,H_2O \qquad [4]$$

In contrast to SO_2 reduction and CO oxidation, the methane oxidation was operating in the kinetic regime

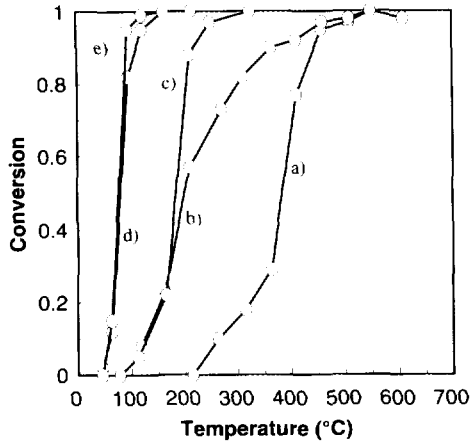

FIG. 8. Catalytic activity for CO oxidation of: (a) precipitated CeO_2, (b) nonstoichiometric CeO_{2-x}, (c) nonstoichiometric La-doped CeO_{2-x}, (d) nonstoichiometric Cu-doped CeO_{2-x}, and (e) precipitated Cu-doped CeO_2.

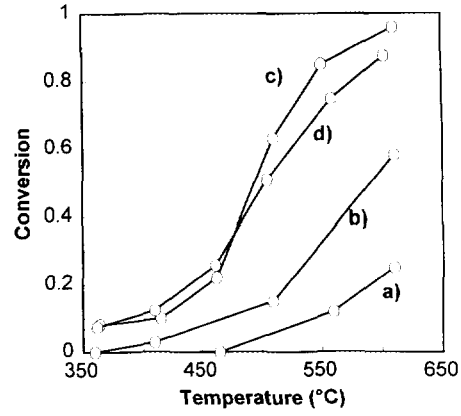

FIG. 10. Catalytic activity in methane oxidation of: (a) precipitated CeO_2, (b) nonstoichiometric CeO_{2-x}, (c) La-doped CeO_{2-x}, and (d) Cu-doped CeO_{2-x} (2% CH_4, 16% O_2, 0.09 s · g/cc (STP)).

under the employed experimental conditions described earlier (7). Therefore, the light-off temperatures varied with contact time and they did not represent the intrinsic kinetic limitation. However, all experiments were performed at the same contact time so that the differences in light-off temperatures were still indicative of the underlying catalytic activities. Pure stoichiometric CeO_2 provided only 20% conversion to the final combustion products even at a temperature of 600°C (Fig. 10). This value was increased to 55% with the use of nonstoichiometric CeO_{2-x}. Further improvement could be achieved with La- and Cu-doping of both types of catalysts. (Figs. 10 and 11).

DISCUSSION

SO_2 Reduction by CO

Cerium oxide is well known for its facile reducibility compared to other fluorite-type oxides. Temperature-programmed reduction (TPR) studies show that surface reduction of precipitated CeO_2 occurs at a maximum rate of about 500°C (33), which is close to the fall-off temperature found for SO_2 reduction. Variation of the nature of dopant cations also reveals a correlation between catalytic activity and oxygen vacancy mobility induced by the dopant (5). These results are interpreted by assuming a redox reaction mechanism for SO_2 reduction by CO as suggested by Happel *et al.* (34) for the same reaction over prereduced $LaTiO_3$ catalysts. The surface of the CeO_2 catalyst is continuously reduced by CO such that oxygen vacancies are created. SO_2 reoxidizes the reduced catalyst surface by donating its oxygen atoms to available vacancies. It is assumed that the reduction process involving several carbonate species is the rate-determining step (5).

The hysteresis found in SO_2 and CO reaction with stoichiometric catalysts indicated the need of prereduction for activation. Furthermore, the active state of the surface was

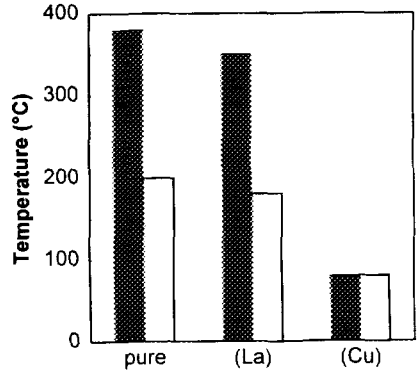

FIG. 9. Temperatures for 50% conversion in CO oxidation for precipitated (full bars) and nonstoichiometric (open bars) catalysts.

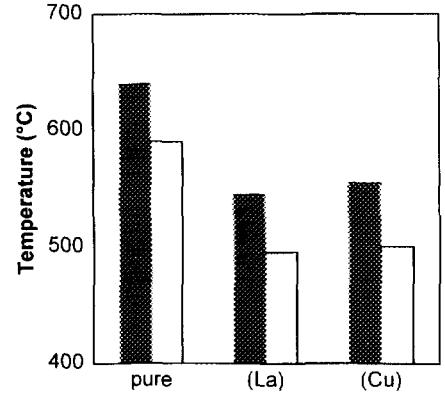

FIG. 11. Reaction temperatures for 50% conversion in methane oxidation for precipitated (full bars) and nonstoichiometric (open bars) catalysts (2% CH_4, 16% O_2, 0.09 s · g/cc (STP)).

completely lost upon the addition of CO_2 into the feed gas stream. Here, the steep drop in sulfur yield was not caused by a simple competition between the two oxidizing species SO_2 and CO_2. Addition of CO_2 changed the reducibility power of the reacting gas mixture. Under overall oxidizing conditions, the surface reduction process ceased and no further CO was oxidized to CO_2. These results could be consistently explained if the active state required a partially reduced surface. The hysteresis was caused by the lack of reduced surface sites on a fully oxidized surface. The initial reduction step required higher thermal activation but once the surface was partially reduced, continuous reduction at a lower activation energy was possible. Under stoichiometric feed composition of reactants the degree of surface reduction was given by the dynamic equilibrium between the rates of the two reactions. However, as excess CO_2 was introduced, all available vacancies were rapidly filled and the surface became oxidized to its initial state. Various carbonate intermediates can be formed when CO_2 adsorbs on a reduced cerium oxide surface. However, the formation of carbonate is not likely to terminate the reaction since CO_2 itself is a reaction product.

The absence of hysteresis in the case of nonstoichiometric materials suggests that the activation process is not necessary or is much easier on a bulk-reduced catalyst. This could be due to the effect of a change in surface oxygen species. In addition to capping oxygen on a CeO_2 surface, a second surface species O_2^- has been identified by ESR (10) and FTIR (11, 35) after oxygen adsorption on prereduced CeO_{2-x}. The existence of this superoxide species is related to the availability of quasi-free electrons in reduced CeO_{2-x}. TPR measurements show that these species are less stable than regular surface-capping oxygen, and are readily available for oxidation reactions at temperatures below 300°C (11, 33). These active species were not part of the catalytic reaction between SO_2 and CO. However, the reaction of O_2^- with CO during activation was important to expose the partially reduced surface before the catalytic reaction could start. Continuous CO_2 admixture in the feed gas during SO_2 reduction oxidized the surface and deactivated the precipitated catalysts, but it could not oxidize the bulk-reduced nonstoichiometric materials to full stoichiometry at temperatures below 500°C. Oxidation of nonstoichiometric CeO_{2-x} in the XPS reaction chamber showed that oxidation did not occur spontaneously, but was thermally activated (Fig. 4) (26). This is also confirmed by TPR measurements, which show that superoxide species are present on bulk-reduced CeO_{2-x} even after oxidation at 300°C (11, 33). Therefore, the effect of nonstoichiometry in CeO_{2-x} on the catalytic activity for SO_2 reduction by CO arose from an abundance of surface oxygen vacancies and a change in surface oxygen species that resulted in lower activation energy for initial surface reduction.

Doping of the CeO_2 catalysts with lanthanum did not increase the catalytic activity in terms of the light-off temperatures for both types of catalytic materials. However, kinetic studies show that La-doping leads to full conversion at shorter contact times. Furthermore, variation in the nature of dopants shows that catalytic activity correlates with oxygen ionic conductivity (5, 6). However, increased concentration of oxygen vacancies through doping did not change the light-off temperature. In contrast, nonstoichiometric CeO_{2-x} catalysts contained oxygen vacancies and quasi-free electrons. The lower light-off and fall-off temperatures and the negligible hysteresis in the nonstoichiometric La-doped CeO_{2-x} must be related to the change in the electronic structure of the material, compared to that of the precipitated sample.

The most active catalyst for SO_2 reduction by CO and for CO oxidation was the Cu-doped cerium oxide, which gave a minor difference in activity in the precipitated and nonstoichiometric forms. It appeared that the promoting effect of Cu dominated the effect of nonstoichiometry, except in the hysteresis behavior during SO_2 reduction by CO. Possible interactions for the promoting effect of Cu include (i) the presence of surface Cu^{1+} as the preferred CO adsorption site, (ii) interstitial Cu^+ in CeO_2 acting as an electron donor and allowing easier CO adsorption even on the CeO_2 surface, and (iii) a change in the enthalpy of vacancy formation due to electronic interaction between Cu and CeO_2 (2). In the first two cases, CO adsorption would be promoted by the availability of electrons, and oxygen vacancies could be created on the CeO_2 surface. A vacancy was either oxidized at its originated site by adsorbed SO_2 species, or diffused from the CO adsorption site and became oxidized elsewhere. Interaction (iii) involves the reducibility of CeO_2. The electronic structure of CeO_2 could be altered by the presence of Cu. Since oxygen vacancy formation involves electron transfer from the valence band to the next available state, thermodynamics of vacancy formation might be changed significantly. A metal oxide that contains doping cations in lower oxidation states has new acceptor levels available. Electronic interaction in the discussions about supported catalysts has usually been limited to metal–semiconductor systems. However, there might also be significant electron transfer at semiconductor–semiconductor junctions resulting in band-bending within CeO_2 (5.5-eV band gap) and Cu_2O (1.5-eV band gap) (36). The relevant interaction would be clarified with the on-going studies on the morphology and chemical state of Cu in CeO_2-based catalysts.

CO Oxidation

In the case of CO oxidation, the most obvious difference from SO_2 reduction is (i) a shift in the light-off temperatures to the range below 200°C for all the nonstoichiometric

CeO_2-based materials and the Cu-doped precipitated CeO_2, and (ii) the absence of any hysteresis effects. This can be explained if CO oxidation proceeds by an extrafacial mechanism between adsorbed oxygen molecules and CO at low temperatures, as reported for V_2O_5 catalysts (37). Formation of oxygen vacancies by CO would no longer be the rate-limiting step if CO could react with adsorbed oxygen rather than lattice oxygen. Variation of the nature of dopants shows no correlation between oxygen vacancy conductivity and catalytic activity, as found in SO_2 reduction (6). This might also indicate the minor role of lattice oxygen and oxygen vacancies in CO oxidation (7). In this case, the higher activity of nonstoichiometric catalysts was caused by the rapid formation of activated ionized surface oxygen species O_2^- due to the availability of free electrons. The catalytic activities for CO oxidation of nonstoichiometric and precipitated Cu-doped catalysts were identical. The promoting effect of Cu on the enthalpy of vacancy formation was not significant in CO oxidation since oxygen vacancies were not involved in this reaction. Therefore, the enhanced catalytic activity of a Cu-doped catalyst must be related to (i) surface Cu which would provide preferred adsorption sites for CO, and/or (ii) interstitial Cu^{1+} which would stabilize Ce^{3+} ions, which in turn enhanced the availability of chemisorbed O_2^- species.

Methane Oxidation

The slope in the activation curve for methane oxidation was rather small compared to those for SO_2 reduction and CO oxidation (see Fig. 10). This reaction was in the kinetic regime under the specified experimental conditions since the light-off temperature varied with contact time (7). However, all experiments were performed at the same contact time of 0.09 g · s/cc (STP). For methane oxidation reaction, the rate-limiting step is assumed to be the breaking of the first C—H bond and the formation of a hydroxyl group. Surface capping oxygen such as O_2^- or O^- species, denoted as [O], can abstract hydrogen from methane by an electrophilic attack on the π bonds (1):

$$[O] + CH_4 \rightarrow OH + CH_3. \qquad [5]$$

The temperature range for this reaction also allows lattice oxygen to participate in the reaction mechanism. For the pure La-doped and Cu-doped materials, the nonstoichiometric catalysts had light-off temperatures 50°C lower than the corresponding stoichiometric precipitated samples. A significant difference between methane oxidation and SO_2 reduction or CO oxidation was apparent in the effect of La- and Cu-doping. In methane oxidation, La-doped catalysts considerably increased activity and were active similarly to the Cu-doped materials, which suggests that dopants can play a major role in methane oxidation.

The enhanced catalytic activity of nonstoichiometric catalysts in all three reactions as compared to the corresponding stoichiometric precipitated materials emphasizes the importance of catalyst electronic and surface oxygen/vacancy properties in oxidation reactions. The unique catalytic activity of the nonstoichiometric cerium oxide stemmed from its mixed conductivity and extensive structural defects as opposed to the pure ionic conductivity and relatively perfect structure of the stoichiometric materials. Doping cerium oxide can possibly result in the same catalyst properties. However, the promoting effect of dopants must be considered in more detail. Doping of the catalyst with Cu or La increased the catalytic activity in all reactions. In the cases of SO_2 reduction and CO oxidation, the Cu-doped catalyst was significantly more active than La-doped catalyst. These two reactions are similar in that CO is the reducing species. In both cases, chemisorption of CO together with formation of carbonate surface species which finally desorb as CO_2 is the rate-limiting step. For methane oxidation, however, La-doped CeO_{2-x} was active similarly to Cu-doped CeO_{2-x}. We may therefore relate the promoting effect of Cu in SO_2 reduction and CO oxidation to the adsorption and surface reaction of CO. Since methane oxidation does not involve CO in its reaction mechanism, the promoting effect of Cu-doping may relate more to oxygen vacancy and electronic effects.

By means of these studies, it was shown that the nature and extent of the effects of nonstoichiometry and dopants in CeO_2-based catalysts could be understood in terms of (i) the presence of superoxide species O_2^- on nonstoichiometric CeO_{2-x}, and (ii) preferred CO adsorption on Cu-doped cerium oxide.

SUMMARY

Nanocrystalline nonstoichiometric pure and doped CeO_2-based catalysts were synthesized by magnetron sputtering and inert gas condensation. Their catalytic activities in SO_2 reduction by CO, CO oxidation, and methane oxidation were investigated and compared with those of stoichiometric chemically precipitated catalysts. The nonstoichiometric materials exhibited increased catalytic activity in all three reactions. For SO_2 reduction by CO, they demonstrated reduced hysteresis in the activity profile and remarkable stability against CO_2 poisoning. These findings could be explained by assuming that the active state of the catalyst involved a partially reduced surface. The higher activity was related to a change in the nature of surface oxygen species for the nonstoichiometric CeO_{2-x}. Superoxide O_2^- was formed on bulk-reduced CeO_{2-x} and was readily available for low-temperature catalytic reactions. This difference translated into easy partial surface reduction, absence of hysteresis, and CO_2 poisoning resistance for the nonstoichiometric catalysts. Catalytic activity could

be modified by doping cerium oxides with La or Cu. La-doping enhanced methane oxidation activity the most, while Cu increased catalytic activity significantly for SO_2 reduction and CO oxidation. The origins of the promoting effect of Cu may be surface and/or electronic interactions, which are being further investigated.

ACKNOWLEDGMENTS

This work was supported by the NSF (CTS-9257223, DMR-9022933), Sloan Funds/MIT, and U.S. DOE (UCR-Program, DE-FG22-92PC92534). Andreas Tschöpe acknowledges fellowship support from the German National Scholarship Foundation (BASF). The authors thank Dr. Michel Trudeau (Materials Research Laboratory, Hydro-Québec, Canada) for his assistance in the XPS studies.

REFERENCES

1. Bielanski, A., and Haber, J., "Oxygen in Catalysis." Dekker, New York, 1991.
2. Boudart, M., and Djéga-Mariadassou, G., "Kinetics of Heterogeneous Catalytic Reactions." Princeton Univ. Press, Princeton, NJ, 1984.
3. Bevan, D. J. M., and Kordis, J., *J. Inorg. Nucl. Chem.* **26,** 1509 (1964).
4. Sørenson, O. T., *J. Solid State Chem.* **18,** 217 (1976).
5. Liu, W., and Flytzani-Stephanopoulos, M., *in* "Environmental Catalysis," (J. N. Armor, Ed.), ACS Symposium Series 552, Chap. 31, p. 375. Am. Chem. Soc., Washington, DC, 1994.
6. Liu, W., Sarofim, A. F., and Flytzani-Stephanopoulos, M., *Appl. Catal. B* **4,** 167 (1994).
7. Liu, W., and Flytzani-Stephanopoulos, M., *J. Catal.* **153,** (1995), in press.
8. Tuller, H. L., and Nowick, A. S., *J. Electrochem. Soc.* **126**(2), 209 (1979).
9. Tuller, H. L., *in* "Nonstoichiometric Oxides" (O. T. Sørenson, Ed.), p. 271. Academic Press, New York, 1981.
10. Che, M., Kibblewhite, J. F. J., Tench, A. J., Dufaux, M., and Naccache, C., *J. Chem. Soc. Faraday Trans.* **69,** 857 (1973).
11. Li, C., Domen, K., Maruya, K., and Onishi, T., *J. Am. Chem. Soc.* **111,** 7683 (1989).
12. Sayle, T. X. T., Parker, S. C., and Catlow, C. R. A., *J. Chem. Soc. Chem. Commun.*, 977 (1992).
13. Gleiter, H., *Prog. Mater. Sci.* **33**(4), 223 (1989).
14. Birringer, R., Herr, U., and Gleiter, H., *Trans. Jpn. Inst. Met.* **27,** 43 (1987).
15. Ying, J. Y., *J. Aerosol Sci.* **24**(3), 315 (1993).
16. Tuller, H. L., and Nowick, A. S., *J. Electrochem. Soc.* **122**(2), 255 (1975).
17. Herman, R. G., Klier, K., Simmons, G. W., Finn, B. P., Bulko, J. B., and Kobylinski, T. P., *J. Catal.* **56,** 407 (1979).
18. Choi, K. I., and Vannice, M. A., *J. Catal.*, **131,** 22 (1991).
19. Tschöpe, A., and Ying, J. Y., *J. Nanostr. Mater.*, **4**(5), 617 (1994).
20. Tschöpe, A., and Ying, J. Y., *in* "Nanophase Materials" (G. C. Hadjipanayis and R. W. Siegel, Eds.), p. 781. Kluwer Academic, Dordrecht/Norwell, MA, 1994.
21. Granqvist, C. G. and Buhrman, R. A., *J. Appl. Phys.* **47**(5) 2200 (1976).
22. Ying, J. Y., *in* "Ceramic Transactions," Vol. 44, p. 67. Am. Ceram. Soc. Westerville, OH, 1994.
23. Kobayashi, T., Haruta, M., Tsubota, S., and Sano, H., *Sens. Actuators B* **1,** 222 (1990).
24. Kochendoerfer, Z., *Kristallogr. Mineral. Petrochem.* **105,** 393 (1944).
25. Cullity, B. D., "Elements of X-ray Analysis," 2nd ed., p. 284. Addison-Wesley, Reading, PA, 1978.
26. Trudeau, M. L., Tschöpe, A., and Ying, J. Y., *Surf. Interface Anal.* **23,** 219 (1995).
27. Subramanian, P. R., and Laughlin, D. E., *in* "Binary Alloy Phase Diagrams" (T. B. Massalski, Ed.), 2nd ed., Vol. 2, p. 1051. ASM International, Materials Park, OH, 1990.
28. Nix, R. M., Rayment, T., Lambert, R. M., Jennings, J. R., and Owen, J., *J. Catal.* **106,** 216 (1987).
29. Laachir, A., Perrichon, V., Badri, A., Lamotte, J., Catherine, E., Lavalley, J. C., El Fallah, J., Hilaire, L., Le Normand, F., Quemere, E., Sauvion, G. N., and Touret, O., *J. Chem. Soc. Faraday Trans.* **87,** 1601 (1991).
30. Tschöpe, A., Ying, J. Y., Amonlirdviman, K., and Trudeau, M. L., *in* "Materials Research Society Symposium Proceedings," Vol. 351, p. 251. Mater. Res. Soc., Pittsburgh, PA, 1994.
31. Le Normand, F., El Fallah, J., Hilaire, L., Legare, P., Kotani, A., and Parlebas, J. C., *Solid State Commun.* **71**(11), 885 (1989).
32. Tschöpe, A., Ying, J. Y., Liu, W., and Flytzani-Stephanopoulos, M., *in* "Materials Research Society Symposium Proceedings," Vol. 344, p. 133. Mater. Res. Soc., Pittsburgh, PA, 1995.
33. Yao, H. C. and Yu Yao, Y. F., *J. Catal.* **86,** 254 (1984).
34. Happel, J., Leon, A. L., Hnatow, M. A., and Bajars, L., *Ind. Eng. Chem. Prod. Res. Dev.* **16**(2), 150 (1977).
35. Ying, J. Y., *in* "Nanophase Materials" (G. C. Hadjipanayis and R. W. Siegel, Eds.), p. 197. Kluwer Academic, Dordrecht/Norwell, MA, 1994.
36. Strehlow, W. H., and Cook, E. L., *J. Phys. Chem. Ref. Data* **2**(1), 163 (1973).
37. Boreskov, G. K., *Kinet. Katal.* **14,** 7 (1973).